

Total-field atomic gradiometer for unshielded portable magnetoencephalography

M. E. Limes, E. L. Foley, and T. W. Kornack
Twinleaf LLC, 300 Deer Creek Dr., Plainsboro, New Jersey, 08536, USA

S. Caliga, S. McBride, and A. Braun
SRI International, 201 Washington Rd., Princeton, New Jersey, 08540, USA

W. Lee, V. G. Lucivero, and M. V. Romalis
Department of Physics, Princeton University, Princeton, New Jersey, 08544, USA
(Dated: November 19, 2021)

Recording of magnetic fields generated by neuronal electrical currents is one of a few available methods for non-invasive functional brain imaging. The fields generated by such currents are about 100 million times smaller than Earth's magnetic field. Most magnetoencephalography (MEG) systems use large magnetic shields to screen Earth's field and magnetic field fluctuations. We present a portable atomic gradiometer that demonstrates unshielded sensitivity of $16 \text{ fT/cm/Hz}^{1/2}$, and use it to detect MEG and magnetocardiography (MCG) signals. The gradiometer uses two cells containing ^{87}Rb vapor that is initially spin-polarized transverse to Earth's field. The ^{87}Rb free-precession frequencies, proportional to the total magnetic field, are measured with a probe laser. Combining state-of-the-art micro-fabricated vapor cells with advanced thermal insulation and custom electronics, we reduce the total system power to 5 W and run the sensor from a laptop. This work demonstrates the possibility of magnetic neuroimaging in a variety of natural environments.

Magnetoencephalography (MEG) and electroencephalography (EEG) serve as important windows into brain function by providing neuronal current source imaging with millisecond resolution, much faster than other noninvasive techniques, such as functional magnetic resonance imaging (fMRI) and positron emission tomography (PET) [1]. MEG in addition has several advantages over EEG, including improved source localization and non-contact measurements [2]. Commercially available MEG systems use superconducting quantum interference device (SQUID) magnetometers or gradiometers with sensitivity of $3\text{--}10 \text{ fT/Hz}^{1/2}$. Existing MEG systems require large installations with magnetically shielded rooms or human-scale magnetic shields as well as dewars and infrastructure for cryogenic operation. Placing subjects in a magnetically shielded room restricts the range of behaviors and activities that can be studied. There are a few demonstrations of MEG detection using SQUIDs in an unshielded environment [3–5], but such recordings rely on third-order gradiometers that are primarily sensitive to shallow neuronal current sources. SQUID gradiometers are fundamentally limited in the cancellation of uniform magnetic fields by the fabrication tolerances of their pick-up coils.

Recently atomic magnetometers have also been used for MEG detection. Most sensitive atomic magnetometers operate using alkali vapors near zero field in a spin-exchange relaxation free (SERF) regime [6]. SERF magnetometers have been used for detection [7–13] and localization [14–16] of MEG signals, but still require magnetic shielding or field cancellation because their operation relies on having a small total magnetic field. In addition, they require individual calibration and have inher-

ently limited linearity and dynamic range. All measurements with wearable SERF magnetometers have been performed so far in magnetically shielded rooms [16, 17].

Here we describe a portable, all-optical atomic gradiometer that can detect MEG signals in Earth's ambient magnetic field, unshielded from natural noise sources. Unlike all previous MEG sensors, we use total-field magnetometers that directly measure the Larmor precession frequency of ^{87}Rb electron spins in the magnetic field. Frequency measurements have a much greater dynamic range and linearity compared to voltage measurements associated with other magnetic field sensors. Furthermore, they do not require individual calibration, so we simply subtract the frequencies recorded from two vapor cells to find the magnetic field gradient. The first-order gradiometer allows detection of deeper current sources.

Total-Field Gradiometer. The gradiometer uses two $8 \times 8 \times 12.5 \text{ mm}^3$ ^{87}Rb vapor cells separated by 3 cm. These cells have anodically bonded glass windows with internal mirrors for 795 nm light [18]. The cells are evacuated, baked, and filled with enriched ^{87}Rb and 650 torr N_2 . In operation they are electrically heated inside of a radiation shield with a low magnetic noise [19]. The cells are attached to a glass substrate with low-thermal-conduction supports and are placed into a $6.5 \times 1.8 \times 1.8 \text{ cm}^3$ cuvette that is evacuated and sealed to maintain high vacuum, eliminating gas conduction and convection. This assembly requires 30 mW/cell to heat to the operating temperature of 100°C , which gives a ^{87}Rb density of about $5 \times 10^{12} \text{ atoms/cm}^3$.

Shown in Fig. 1, the gradiometer is oriented such that multi-pass laser beams are perpendicular to Earth's field $B_E = 51.4 \mu\text{T}$. ^{87}Rb atoms are polarized by an on-

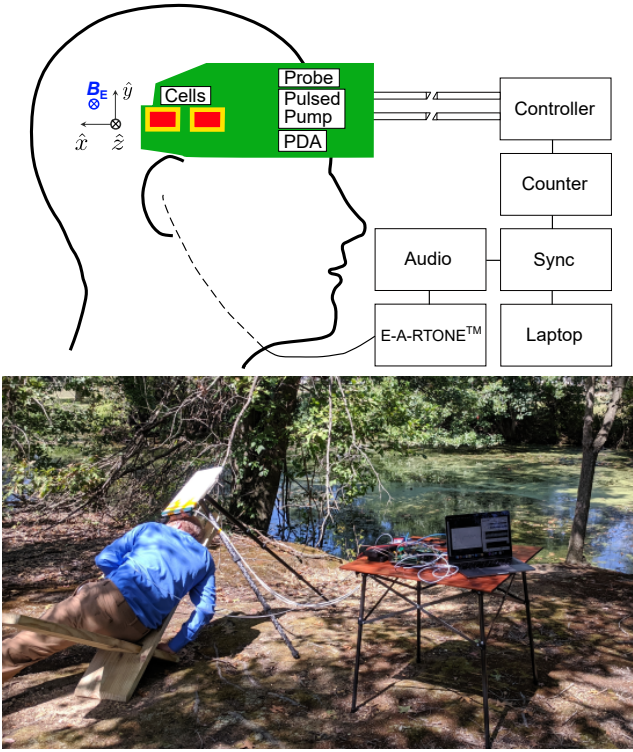


FIG. 1. *Schematic and picture of apparatus.* Top: Two vacuum-packaged ^{87}Rb vapor cells are placed near a subject's auditory cortex and measure the total field gradient dB_z/dx with a 3 cm baseline. The Rb vapor is optically pumped and probed by diode lasers integrated into the sensor. Optical rotation of the probe laser is detected with a photodiode amplifier (PDA). The sensor is controlled by compact electronics including a custom counter that streams Rb Larmor frequencies to the laptop. Bottom: A picture of the recording setup with a subject.

resonant (D1) pulsed pump diode laser that is able to produce several W for μs pulses. The beam is sent through a polarizer and $\lambda/4$ wave plate to make σ^+ light for optical pumping. We use a style of optical pumping similar to a conventional Bell-Bloom scheme [20, 21], though we use a pumping state initialization period followed by a free-precession detection period in order to eliminate frequency shifts associated with the pump laser. We pump ^{87}Rb atomic spins in the transverse plane to near unity polarization, which causes a suppression of the dominant spin-exchange relaxation mechanism between the $F = 2$ and $F = 1$ hyperfine manifolds at these sizable magnetic fields, and leads to an extension in ^{87}Rb coherence time T_2 [22, 23]. A 0.1 mW linearly polarized VCSEL probe beam is far-detuned from resonance (D1) and undergoes paramagnetic Faraday rotation in a multi-pass configuration that yields high signal-to-noise [24–26]. The probes of each cell are sent into balanced polarimeters that measure signals from ^{87}Rb free precession about the total field. The entirety of the optics and lasers are housed in a 3D-printed case along with a photodiode amplifier

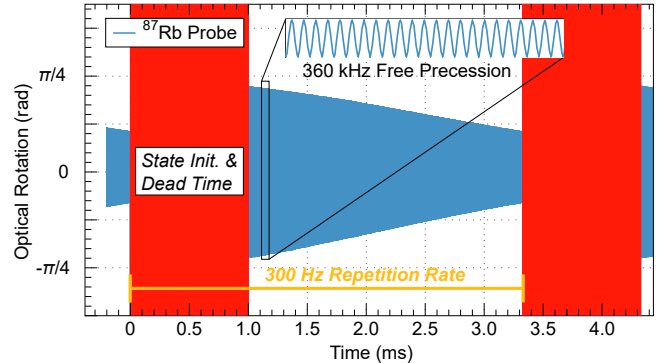


FIG. 2. *Operation of total-field atomic gradiometer.* Each vapor cell has ^{87}Rb optically pumped to near unity polarization and is probed during its free precession about a total field B_E . A custom frequency counter detects signal zero crossings in the free precession interval, and extracts a field by dividing by the ^{87}Rb gyromagnetic ratio $\gamma \approx 7 \text{ kHz}/\mu\text{T}$. The two fields detected for each cell are streamed to a laptop at a data rate of 300 Hz.

(PDA) board. Although detection of free precession is in principle a calibration-free measurement of the field that each cell experiences, its absolute accuracy is affected to some degree by heading errors, light shifts due to any remnant circular polarization of the probe laser, as well as any remnant magnetization of the components used in the sensor construction. Some of these effects can be minimized by aligning the lasers transverse to the total field B_z . Such DC offsets do not affect detection of MEG signals.

The electronics for the gradiometer consist of two $6.4 \times 12.7 \text{ cm}^2$ PCB boards each powered by 2.5 W from a USB laptop port (or a 5V battery). One board controls the sensor heating and probe laser, while the other contains a frequency counter and controls the pump pulse sequence. The frequency counter streams two timestamped frequencies to a Labview VI for real-time analysis and logging. The sensitivity of the frequency counter is shown in Supplementary Fig. 1. The magnetic field gradient is calculated by taking the differences of the frequencies and dividing by the ^{87}Rb gyromagnetic ratio $\gamma = 7 \text{ kHz}/\mu\text{T}$. The power consumption of the boards is dominated by the microcontrollers and can be reduced with available lower-power versions. A sample ^{87}Rb free precession signal is shown in Fig. 2. We use a shot-to-shot repetition rate of 300 Hz and after 1 ms of state initialization and dead time, our acquisition time is 2.3 ms per shot.

RESULTS

In-the-field MEG. To study auditory evoked field responses, 1 kHz audio stimuli of duration 50 ms is generated with the delivery time randomized in a $2.5 \pm 1 \text{ s}$

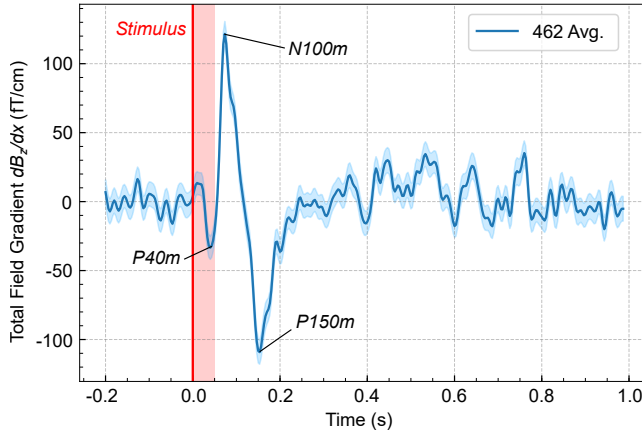


FIG. 3. Auditory evoked fields detected unshielded in Earth's field. Filtered average of 462 epochs is shown for dB_z/dx gradient data taken above a subject's right ear, while a time-randomized 1 kHz audio beep is introduced into their left ear. Bands indicate the standard error of the mean. The auditory evoked fields observed include the prominent N100m peak along with indication of P40m and P150m responses.

window to prevent subject adaptation. The stimuli are delivered by a non-magnetic pneumatic earphone. The gradiometer is held by a non-magnetic mount near the audio cortex above the opposing ear, as the subject rests in a wooden chair. The center of each cell is about 1.2 cm away from the head of the subject, smaller than the typical distance for SQUID magnetometers. A synchronization board is used to ensure the precise time-stamping of the audio stimuli and the gradiometer data. The gradiometer is oriented to optimize the signal for a current dipole expected for auditory evoked responses. Auditory evoked field data was recorded for four subjects in several 5-20 min trials, using different sensor positions and orientation.

We show in Fig. 3 MEG data filtered and averaged over 462 epochs for a subject in a trial. For data analysis we apply a 0.5-50 Hz bandpass filter, along with 25, 60, and 120 Hz notch filters, and observe P40m, N100m, and P150m evoked fields (the response observed at 150 ms here is likely the typically reported P200 response [27, 28]). Auditory evoked signals were detected in all four subjects and the sign of the detected dB_z/dx peaks is consistent with the orientation of the current dipole observed in previous studies of auditory evoked fields. The orientation of the sensor and head with respect to the Earth's field is critical, as total-field magnetometers are only sensitive to the component of the evoked field parallel to the bias field. Field changes in the transverse plane B_T appear only in second order $B_T^2/2B_E$ and are negligible. Additional MEG data and analysis are shown in Supplementary Fig. 2, 3, 4.

In Fig. 4 we show a representative spectral density of the gradiometer noise with a subject present. We obtain

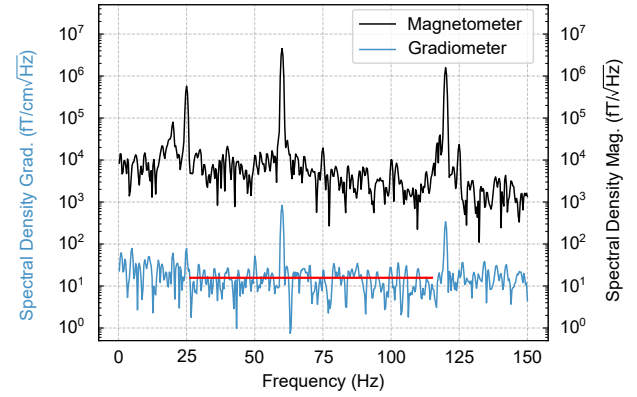


FIG. 4. Unshielded total-field gradiometer performance in Earth's field. Spectral densities with a subject for gradiometer and magnetometer (single ^{87}Rb vapor cell) data. The red line is a fit to the noise floor giving $15.7 \text{ fT}/\text{cm}\sqrt{\text{Hz}}$.

a similar noise level measured without a subject. We also show the spectral density of single-channel magnetometer measurements. The 60 and 120 Hz components are the largest peaks observed, coming from power lines roughly 75 m away. Another prominent peak at 25 Hz comes from a nearby New Jersey Transit/Amtrak Rail line about 750 m away. Considering the 3 cm baseline, the 60 Hz peak suppression of the gradiometer indicates a common mode rejection ratio of at least 2000. It is difficult to separate real gradient noise from the intrinsic noise floor of the gradiometer in an unshielded environment without multiple gradiometers. The gradiometer spectral density between 26 and 115 Hz ignoring 50 and 60 Hz peaks gives $15.7 \text{ fT}/\text{cm}\sqrt{\text{Hz}}$; this implies a magnetometer noise floor of $50 \text{ fT}/\sqrt{\text{Hz}}$, outperforming commercially available scalar atomic sensors operating unshielded in Earth's field. Within magnetic shielding, the total-field gradiometer achieves $10 \text{ fT}/\text{cm}\sqrt{\text{Hz}}$ with a field of $50 \mu\text{T}$ applied, as shown in Supplementary Fig. 5.

We briefly mention that another important medical application of sensitive magnetometers is magnetocardiography (MCG). Magnetic fields generated by the heart are stronger, but their detection in unshielded environment remains a challenge. A number of optically-pumped sensors are being developed for this application [29–32]. Here we show real-time in-the-field MCG signals in Fig. 5 that are taken by simply walking up and presenting the chest to the sensor, along with a 10 s averaging of human heartbeats. Even in its current form our sensor is not far from providing a practical MCG device that allows quick, electrode-free heart diagnostics for triage in ambient environments.

We have shown a proof-of-principle detection of unshielded MEG and MCG signals using a portable total-field first-order gradiometer. Wearable atomic sensors that do not require shielding will enable a greater vari-

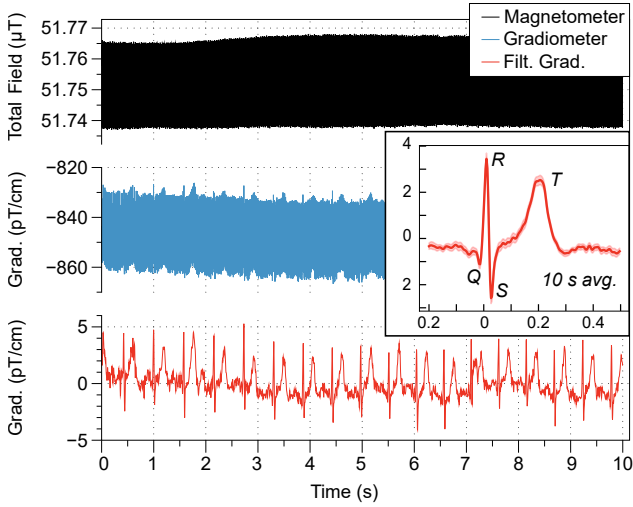


FIG. 5. Demonstration of in-the-field MCG data. Top panel - raw magnetometer signal, middle panel- raw gradiometer signal, bottom panel - gradiometer signal with a real-time filter (bandpass 0.1-50 Hz, notch at 60/120 Hz) showing a human heartbeat. The inset shows averaging data of 10 s, triggered on R peak.

ety of MEG research studies, as well as reduce their cost. They can eventually replace EEG sensors currently being used in a variety of open-source EEG systems [33]. By using an all-optical design we have eliminated cross-talk between sensors, which will allow one to build a gradiometer array. Such an array is necessary to suppress magnetic gradient noise from power lines and other nearby sources, enabling operation in a typical lab or hospital environment. The sensitivity of the gradiometer can be further improved [25]. We believe the development of cost-effective sensors that can be used in an array will impact the scope of many MEG and MCG studies, as well as the various other applications that can benefit from a commercially available sensor for total-field magnetometry in Earth's field.

DATA AVAILABILITY

The data and code that support the findings of this study are available from the corresponding author on reasonable request.

[1] M. Hämäläinen, R. Hari, R. J. Ilmoniemi, J. Knuutila, and O. V. Lounasmaa, *Rev. Mod. Phys.* **65**, 413 (1993).
[2] S. Baillet, *Nature Neuroscience* **20**, 327 EP (2017), review Article.
[3] J. Vrba, B. Taylor, T. Cheung, A. A. Fife, G. Haid, P. R. Kubik, S. Lee, J. McCubbin, and M. B. Burbank,

IEEE Transactions on Applied Superconductivity **5**, 2118 (1995).

[4] Y. Okada, K. Pratt, C. Atwood, A. Mascarenas, R. Reineman, J. Nurminen, and D. Paulson, *Review of Scientific Instruments* **77**, 024301 (2006), <https://doi.org/10.1063/1.2168672>.
[5] Y. Seki, A. Kandori, K. Ogata, T. Miyashita, Y. Kumanai, M. Ohnuma, K. Konaka, and H. Naritomi, *Review of Scientific Instruments* **81**, 096103 (2010), <https://doi.org/10.1063/1.3482154>.
[6] I. K. Kominis, T. W. Kornack, J. C. Allred, and M. V. Romalis, *Nature* **422**, 596 (2003).
[7] H. Xia, A. Ben-Amar Baranga, D. Hoffman, and M. V. Romalis, *Applied Physics Letters* **89**, 211104 (2006), <https://doi.org/10.1063/1.2392722>.
[8] C. Johnson, P. D. D. Schwindt, and M. Weisend, *Applied Physics Letters* **97**, 243703 (2010), <https://doi.org/10.1063/1.3522648>.
[9] T. H. Sander, J. Preusser, R. Mhaskar, J. Kitching, L. Trahms, and S. Knappe, *Biomed. Opt. Express* **3**, 981 (2012).
[10] C. N. Johnson, P. D. D. Schwindt, and M. Weisend, *Physics in Medicine and Biology* **58**, 6065 (2013).
[11] V. K. Shah and R. T. Wakai, *Physics in Medicine & Biology* **58**, 8153 (2013).
[12] O. Alem, A. M. Benison, D. S. Barth, J. Kitching, and S. Knappe, *Journal of Neuroscience* **34**, 14324 (2014), <https://www.jneurosci.org/content/34/43/14324.full.pdf>.
[13] J. Sheng, S. Wan, Y. Sun, R. Dou, Y. Guo, K. Wei, K. He, J. Qin, and J.-H. Gao, *Review of Scientific Instruments* **88**, 094304 (2017), <https://doi.org/10.1063/1.5001730>.
[14] K. Kim, S. Begus, H. Xia, S.-K. Lee, V. Jazbinsek, Z. Trontelj, and M. V. Romalis, *NeuroImage* **89**, 143 (2014).
[15] E. Boto, S. S. Meyer, V. Shah, O. Alem, S. Knappe, P. Kruger, T. M. Fromhold, M. Lim, P. M. Glover, P. G. Morris, R. Bowtell, G. R. Barnes, and M. J. Brookes, *NeuroImage* **149**, 404 (2017).
[16] E. Boto, N. Holmes, J. Leggett, G. Roberts, V. Shah, S. S. Meyer, L. D. Muñoz, K. J. Mullinger, T. M. Tierney, S. Bestmann, G. R. Barnes, R. Bowtell, and M. J. Brookes, *Nature* **555**, 657 EP (2018).
[17] R. M. Hill, E. Boto, N. Holmes, C. Hartley, Z. A. Seedat, J. Leggett, G. Roberts, V. Shah, T. M. Tierney, M. W. Woolrich, C. J. Stagg, G. R. Barnes, R. R. Bowtell, R. Slater, and M. J. Brookes, *Nature Communications* **10**, 4785 (2019).
[18] N. Dural and M. V. Romalis, “Anodically bonded cells with optical elements,” (2017), uS Patent 10345548.
[19] H. B. Dang, A. C. Maloof, and M. V. Romalis, *Applied Physics Letters* **97**, 151110 (2010), <https://doi.org/10.1063/1.3491215>.
[20] W. E. Bell and A. L. Bloom, *Physical Review Letters* **6**, 280 (1961).
[21] V. Gerginov, S. Krzyzewski, and S. Knappe, *J. Opt. Soc. Am. B* **34**, 1429 (2017).
[22] M. V. Romalis, H. Dong, and A. Baranga, “Us 20180356476a, pulsed scalar atomic magneometer,” (2018).
[23] V. G. Lucivero and M. V. Romalis, In preparation.
[24] S. Li, P. Vachaspati, D. Sheng, N. Dural, and M. V. Romalis, *Phys. Rev. A* **84**, 061403 (2011).
[25] D. Sheng, S. Li, N. Dural, and M. V. Romalis, *Phys. Rev. Lett.* **110**, 160802 (2013).

- [26] W. Lee and M. V. Romalis, In preparation.
- [27] J. P. Mäkelä, A. Ahonen, M. Hämäläinen, R. Hari, R. Llmoniemi, M. Kajola, J. Knuutila, O. V. Lounasmaa, L. McEvoy, R. Salmelin, O. Salonen, M. Sams, J. Simola, C. Tesche, and J.-P. Vasama, *Human Brain Mapping* **1**, 48 (1993).
- [28] A. Gutschalk, “Meg auditory research,” in *Magnetoencephalography: From Signals to Dynamic Cortical Networks*, edited by S. Supek and C. J. Aine (Springer International Publishing, Cham, 2019) pp. 907–941.
- [29] G. Bison, R. Wynands, and A. Weis, *Opt. Express* **11**, 904 (2003).
- [30] R. Wyllie, M. Kauer, R. T. Wakai, and T. G. Walker, *Opt. Lett.* **37**, 2247 (2012).
- [31] O. Alem, T. H. Sander, R. Mhaskar, J. LeBlanc, H. Eswaran, U. Steinhoff, Y. Okada, J. Kitching, L. Trahms, and S. Knappe, *Physics in Medicine & Biology* **60**, 4797 (2015).
- [32] M. Bai, Y. Huang, G. Zhang, W. Zheng, Q. Lin, and Z. Hu, *Optics Express* **27**, 29534 (2019).
- [33] OpenBCI, <https://openbci.com//>.

ACKNOWLEDGEMENTS

This work was funded by the Defense Advanced Research Projects Agency (DARPA) Microsystems Technology Office (MTO) under Contract No. 140D6318C0020. The views, opinions and/or findings expressed are those of the authors and should not be interpreted as representing the official views or policies

of the Department of Defense or the U.S. Government. Approved for Public Release, Distribution Unlimited.

CONTRIBUTIONS

M.E.L., T.W.K. operated sensor and analyzed data. E.L.F. aligned optics in sensor and filled anodically bonded cells. S.C., S.M., designed and built low-power vapor-cell assembly. T.W.K. designed custom electronics and software for portable operation. W.L., V.G.L., M.V.R. determined optimal operating parameters for sensor. A.B., M.V.R., E.L.F., T.W.K. conceived and supervised overall project. M.E.L., M.V.R. prepared this manuscript with contributions from all authors.

CORRESPONDING AUTHORS

Correspondence to Mark Limes (limes.mark@gmail.com), Tom Kornack (kornack@twinleaf.com), Mike Romalis (romalis@princeton.edu), or Alan Braun (alan.braun@sri.com).

COMPETING INTERESTS

The authors declare no competing interests.

SUPPLEMENTARY INFORMATION

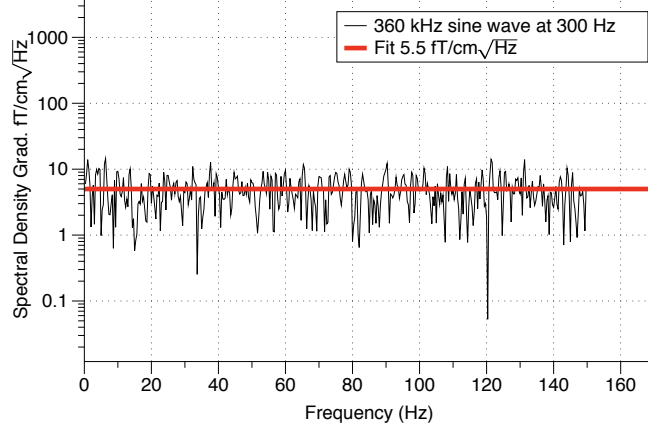


FIG. 1. The custom frequency counter is set up under the operating conditions used in the main text, triggered on 300 Hz and acquisition window of 2.3 ms. 360 kHz sine waves from a function generator are sent into the two channels. A fit to the white noise gives our reported portable detection noise floor of $5.5 \text{ fT/cm}\sqrt{\text{Hz}}$.

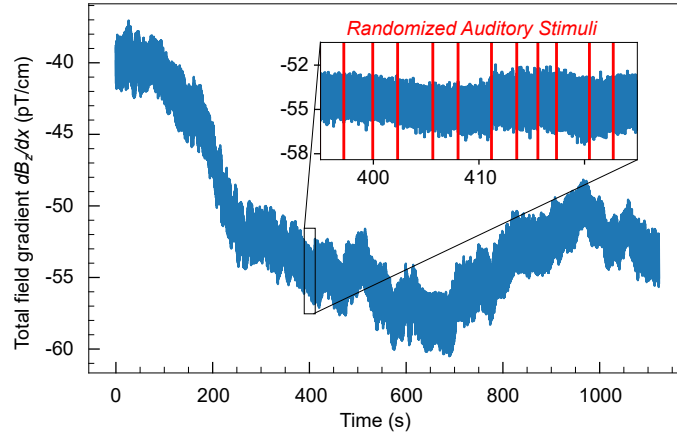


FIG. 2. The raw dB_z/dx gradient data shown averaged in Fig. 3 of the main text.

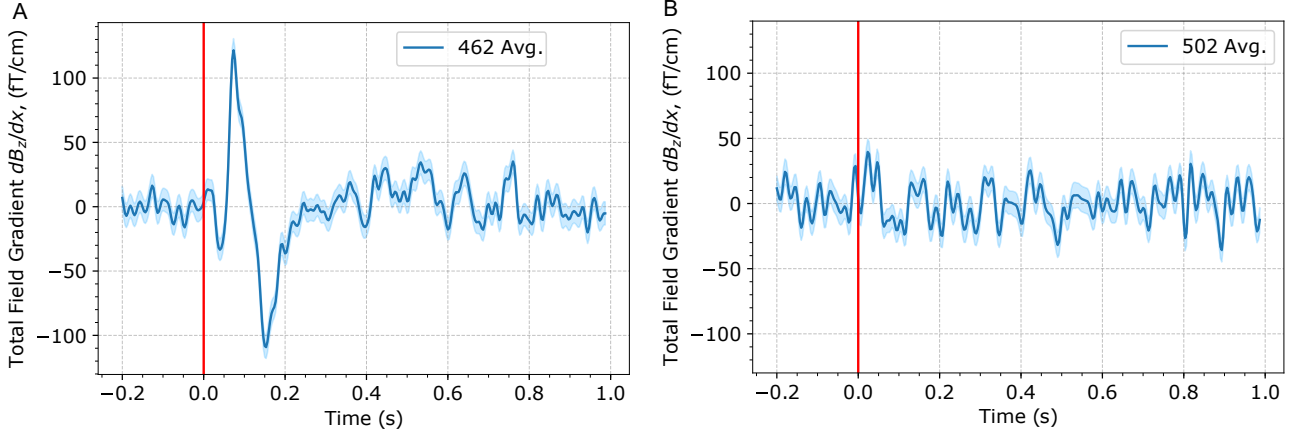


FIG. 3. Data for subject with (A) and without (B) auditory stimuli.

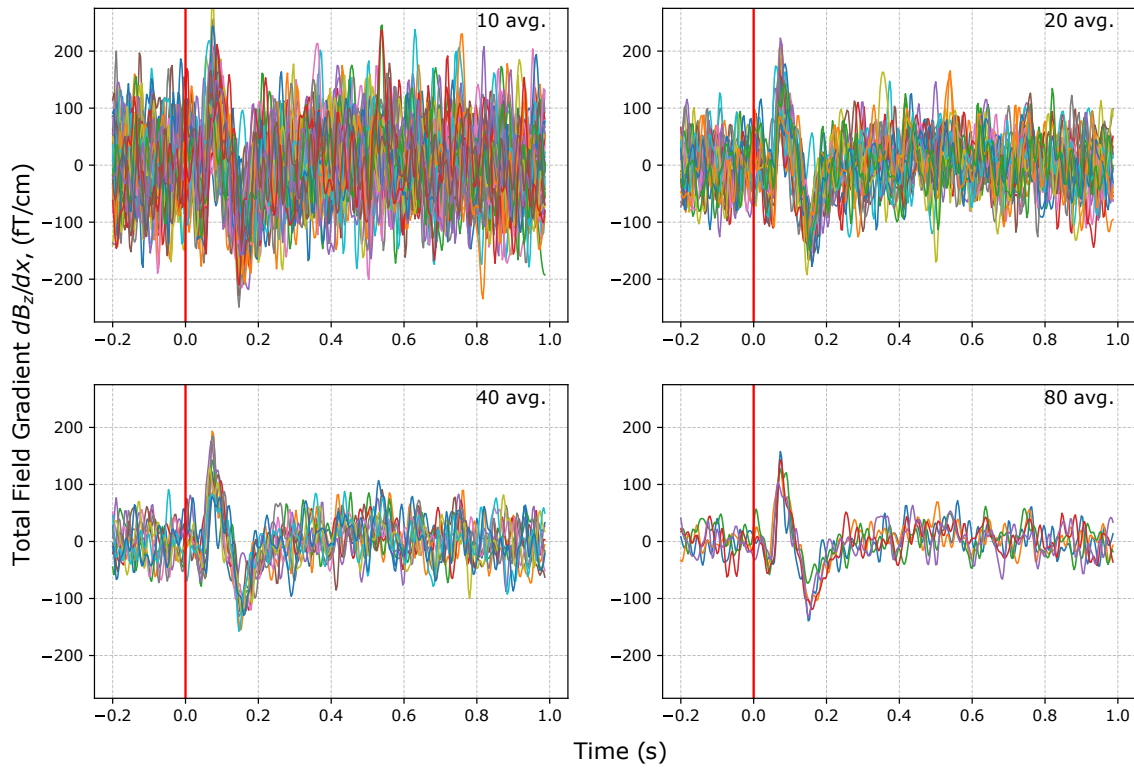


FIG. 4. Taking averages (10, 20, 40, and 80) of the data taken shown in Fig. 3 of the main text.

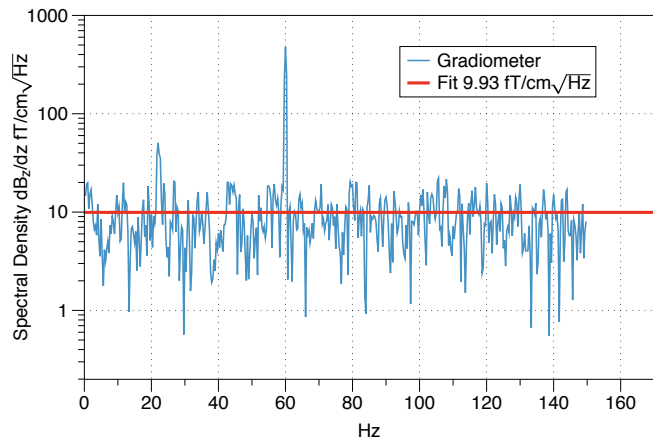


FIG. 5. Spectral density of gradiometer in magnetic shielding (Twinleaf MS-2), taken with $49.3 \mu\text{T}$ bias field.